Mechanical Properties of the Proton from a Deformed AdS Holographic Model

Ayrton Nascimento^{1*} and Henrique Boschi-Filho^{1†}

¹Instituto de Física, Universidade Federal do Rio de Janeiro,
21.941-909, Rio de Janeiro, RJ, Brazil

We study the gravitational form factors of the proton and some of its mechanical properties. We use a holographic model based on the AdS/CFT correspondence, in which a deformation in the anti-de Sitter background geometry is considered. By describing the proton as a Dirac field in this background, we numerically evaluate the gloun contribution of its gravitational form factors A and C from its energy-momentum tensor. A comparison of our numerical results with respect to some lattice QCD results and previous results in holography is made. In general, a good agreement is found. We also evaluate the term D and make use of it to compute the pressure and shear distributions in the system, which result in a stable composed particle interpretation consistent with the von Laue stability condition. The energy distribution in the system is also obtained. Internal forces are investigated to support this picture. We are also able to compute the radii associated with these distributions in the proton.

Keywords: Form factors, gauge-gravity duality, holography, hadron structure.

^{*} ayrton@pos.if.ufrj.br

[†] boschi@if.ufrj.br

I. INTRODUCTION

The proton, one of the building blocks of nuclear matter and, consequently, ordinary stuff, has been known for more than one century; however, some of its properties remain at least partially unknown. This is due mainly to its internal structure with non-trivial contributions from its constituents, the quarks and gluons. One way to address this endeavor is to look at the Energy Momentum Tensor's (EMT) gravitational form factors (GFFs), which encode information regarding the distribution of its mass or momentum, spin, shear, and pressure. This question naturally expands to nucleons and other hadrons [1–5]. In principle, GFFs can be probed by the gravitational interaction of quarks and gluons with the graviton, but this constitutes a challenging experimental effort because of the weakness of the gravitational interaction at the quantum level. This was proposed long ago by Gell-Mann 6. Recently, experimental extractions of GFFs have been performed indirectly, for instance, accessing them through deep virtual Compton scattering data [1, 7]. The future Electron Ion Collider [8] looks to further extend such experimental investigations using scattering processes to extract GFFs and to investigate the nucleon structure and its properties. On the theory side, recent developments in lattice QCD, such as [9–12], explored proton GFFs and some of its mechanical properties, such as pressure and shear distributions.

As non-perturbative aspects of QCD related to its strong coupling regime, such properties of the nucleon are also well suited for holographic models based on the gauge/gravity duality [13–15], which relates a classical weakly coupled gravity theory on a curved five dimensional anti-de Sitter space to a dual strongly coupled gauge theory on flat Minkowski space. In this context, the works of [16–36] paved the way for studies of nucleon and hadronic GFFs and some of their mechanical properties such as those mentioned above using holographic models for QCD, also known as AdS/QCD models. Among these models, we mention the hard wall [37–42], the soft wall [43–46], which are classified as bottom-up models, as well as some top-down models such as the D4-D8 Sakai-Sugimoto [47–49]. The role of confinement in the soft wall model inspired [50] another bottom-up AdS/QCD model known as the deformed AdS [51–54]. A comparison remarking similarities and differences of soft wall and deformed AdS models appeared recently in [55].

In this work, we explore the proton gravitational form factors by computing the eigen values of the nucleon EMT in a deformed AdS background holographic model [51–54]. One

of them, the D term, allows one to explore mechanical properties of the system such as pressure and shear distributions, as well as internal forces.

This paper is organized as follows. In Section II, we describe the holographic model used in this work and how to describe the nucleon as a Dirac field on this background. Section III is devoted to the computation of the gravitational form factors of the nucleon, and the comparison of our results with some lattice QCD data, as well as with the holographic results of [27]. From these, in Section IV, we explore the pressure, shear, and energy distributions in the nucleon using a dipole approximation to our numerical results, which also allows us to compute the mechanical radius associated with these distributions. Using these results, in Section V, we investigate the internal forces in the proton, such as normal and tangential forces inside of it. We draw our conclusions and future perspectives in Section VI.

II. HOLOGRAPHIC MODEL

In the deformed AdS model, we consider a five-dimensional anti-de Sitter background deformed by a warp factor $\mathcal{A}(z)$ as follows [54, 55]

$$ds^{2} = g_{mn} dx^{m} dx^{n} = e^{2 A(z)} (dz^{2} + \eta_{\mu\nu} dy^{\mu} dy^{\nu}), \tag{1}$$

where $\{m, n\}$ refers to coordinates in five dimensions, and $\eta_{\mu\nu}$ is the Minkowski metric with signature (-, +, +, +). The warp factor $\mathcal{A}(z)$ is separated into two parts,

$$\mathcal{A}(z) = -\log z + \frac{1}{2}kz^2,\tag{2}$$

where $-\log z$ refers to the asymptotic background $z \to 0$ AdS₅, with radius of curvature R = 1, which, in the bulk, is deformed by a dilaton-like factor of $\frac{1}{2}kz^2$, with k a constant having a mass squared dimension. The extra term in the deformed AdS background is responsible for breaking the conformal invariance of the boundary quantum field theory. It was originally chosen to reproduce confining quark-antiquark potentials [50].

A. Proton in the deformed AdS background

Fermions, such as the proton, are described by a probe Dirac field Ψ in five dimensions [54, 55]

$$S = \int dz \, d^4x \, \sqrt{-g} \, \bar{\Psi}(\not \!\!\!D - m_5) \Psi, \tag{3}$$

where g is the determinant of the metric of the bulk geometry (1), and m_5 is the bulk fermionic mass. The operator $\not D$ is defined by

$$D \equiv g^{mn} e_n^a \Gamma_a \left(\partial_m + \frac{1}{2} \omega_m^{bc} \Sigma_{bc} \right), \tag{4}$$

where $\Sigma_{bc} = \frac{1}{4}[\Gamma_b, \Gamma_c]$, with Dirac matrices given by $\Gamma^a = (\gamma^\mu, -i\gamma^5)$. The vielbein e_n^a for the deformed background is

$$e_m^a = e^{\mathcal{A}(z)} \, \delta_m^a. \tag{5}$$

The spin connection ω_m^{bc} is

$$\omega_m^{ab} = e_n^a \,\partial_m e^{nb} + e_n^a \,e^{pb} \,\Gamma_{pm}^n, \tag{6}$$

where m = 0, 1, 2, 3, 5, and Γ_{pm}^n are the Christoffel symbols

$$\Gamma_{mn}^{p} = \frac{1}{2} g^{pq} (\partial_n g_{mq} + \partial_m g_{nq} - \partial_q g_{mn}). \tag{7}$$

From (3), one can get the following equation of motion

$$(e^{-\mathcal{A}(z)}\gamma^5\partial_z + e^{-\mathcal{A}(z)}\gamma^\mu\partial_\mu + 2\mathcal{A}'(z)\gamma^5 - m_5)\Psi = 0,$$
(8)

with A'(z) denoting the derivative with respect to the holographic coordinate z. We can decompose Ψ into left e right chiral components

$$\Psi(x^{\mu}, z) = \Psi_{L}(x^{\mu}, z) + \Psi_{R}(x^{\mu}, z),, \tag{9}$$

with $\Psi_{L/R} = \frac{1 \mp \gamma^5}{2} \Psi$. Considering that the Kaluza-Klein modes are dual to the chiral components, one can write them as

$$\Psi_{L/R}(x,z) = \sum_{n} f_{L/R}^{n}(x) \chi_{L/R}^{n}(z). \tag{10}$$

Using (9) and (10) in (8), we get the following system of coupled equations

$$(\partial_z + 2 A'(z) e^{A(z)} + m_5 e^{A(z)}) \chi_L^n(z) = M_n \chi_R^n(z),$$
(11)

$$(\partial_z + 2 \mathcal{A}'(z) e^{\mathcal{A}(z)} - m_5 e^{\mathcal{A}(z)}) \chi_R^n(z) = -M_n \chi_L^n(z), \tag{12}$$

with M_n the mass of the *n*th excited state. By decoupling these equations and using the following transformations,

$$\chi_{L/R}^n(z) = \psi_{L/R}^n(z) e^{-2A(z)},$$
(13)

	ψ_L	ψ_R
M_0	$0.937801 \mathrm{GeV^2}$	$0.937135\mathrm{GeV}^2$

Table I: Masses of the chiral solutions ψ_L and ψ_R for $k = (0.343)^2 \text{ GeV}^2$ and $\gamma = 1.745$.

we obtain a Schrödinger-like equation for the fermions

$$[-\partial_z^2 + V_{L/R}(z)] \psi_{L/R}^n(z) = M_n^2 \psi_{L/R}^n(z), \tag{14}$$

where the corresponding chiral potentials are given by

$$V_{L/R}(z) = m_5^2 e^{2A(z)} \mp e^{A(z)} m_5 A'(z).$$
 (15)

In order to model gravitational form factors, we need to solve (14) for its ground state. With $\mathcal{A}(z)$ given by (2), the resulting fermionic solution is obtained by numerically solving the Schrödinger-like equation. The goal is to make the ground state mass M_0 match the proton mass of $M_p = 0.938 \,\text{GeV}^2$. We seek for free parameters to achieve this goal. The constant k present in the background warp factor $\mathcal{A}(z)$ can be fine tuned along with the bulk mass m_5 , given by

$$m_5 = \Delta - 2, \tag{16}$$

where Δ is the fermionic conformal dimension $\Delta = \frac{3}{2}$ [54, 55]. With the resulting value of m_5 we are unable to reproduce the mass of the proton for any chosen value of k. For this purpose, we use an anomalous dimension γ such that

$$m_5 = \Delta + \gamma - 2. \tag{17}$$

In this way, we can fine tune both parameters, k and γ , to not only match M_0 with the proton mass, but to adjust the predictions of this model for the gravitational form factors of the proton with the corresponding results in the lattice QCD literature, and compare them with previous holographic results. As we shall see in the next section, the values that best achieve this goal are found to be $k = (0.343)^2 \,\text{GeV}^2$ and $\gamma = 1.745$, as illustrated by the masses of the ψ_L e ψ_R solutions in Table I.

III. GRAVITATIONAL FORM FACTORS

The mechanical properties of matter are related to the way in which it interacts with gravitational fields [5]. The response of gravity to the presence of matter is translated into the energy-momentum tensor (EMT) such that matter mechanical properties can be extracted from its matrix elements between single particle states in terms of form factors. The general decomposition of QCD EMT in terms of gravitational form factors is given by [2, 27, 30]

$$\langle p_2 | T^{\mu\nu}(0) | p_1 \rangle = \bar{u}(p_2) \left(A(q) \, \gamma^{(\mu} p^{\nu)} + B(q) \, \frac{i \, p^{(\mu} \sigma^{\nu)\alpha} q_\alpha}{2 \, m_N} + C(q) \, \frac{q^\mu q^\nu - \eta^{\mu\nu} q^2}{m_N} \right) u(p_1), \quad (18)$$
 with $a^{(\mu} b^{\nu)} = \frac{1}{2} (a^\mu b \nu + a^\nu b^\mu), \quad q^2 = (p_2 - p_1)^2$ and $\bar{u}u = 2 \, m_N$, with m_N the nucleon mass. The scalar coefficients A, B , and C are the gravitational form factors, which encode information on momentum distribution, spin and angular momentum, as well as internal mechanical forces distributions inside the nucleon, respectively.

The energy-momentum tensor can be obtained by varying the action coupled to classical gravity with respect to the metric $g^{\mu\nu}$

$$T^{\mu\nu}(x) = \frac{2}{\sqrt{-g}} \frac{\delta S_{\text{grav}}}{\delta g^{\mu\nu}(x)},\tag{19}$$

In holography, the EMT sources a fluctuation in the bulk metric such that

$$g_{MN}(z) \to g_{MN}(z) + h_{MN}(z), \tag{20}$$

with line element given by (1), and warp factor $\mathcal{A}(z) = -\log z + k z^2/2$. The form factors are obtained by coupling the metric fluctuation h_{MN} to the Dirac fermions $\psi_{L/R}$ present in the bulk EMT. To reproduce its tensorial structure in (18), we decompose the metric fluctuation into a transverse-traceless part h(q, z), and a longitudinal trace full part H(q, z)

$$h_{MN}(q,z) = \epsilon_{MN}^{TT} h(q,z) + q_M q_N H(q,z).$$
 (21)

In the axial gauge $h_{Mz} = h_z z = 0$, the corresponding graviton equation of motion obtained from the linearized Einstein's equations takes the form of

$$\frac{1}{\sqrt{-g}} \,\partial_M(\sqrt{-g} \,g^{MN} \partial_N \,h_{\mu\nu}) = 0. \tag{22}$$

By numerically solving this last equation for each component of $h_{\mu\nu}$, one can obtain the form factors using (3) as the bulk gravitational action in (19). As a consequence of this choice, one can show that there will be no coupling between metric fluctuation and a spin term σ^{μ} in the deformed AdS model, resulting in a vanishing B form factor.

A. $A(q^2)$ form factor

The $A(q^2)$ form factor is obtained by contracting (18) with $\epsilon_{\mu\nu}^{TT}$

$$\langle p_2 | \epsilon_{\mu\nu}^{TT} T^{\mu\nu} | p_1 \rangle = \bar{u}(p_2) A(q) \epsilon_{\mu\nu}^{TT} \gamma^{\nu} p^{\nu} u(p_1),$$
 (23)

where

$$A(q^2) = \frac{1}{2} \int dz \, e^{-5\mathcal{A}(z)} (\psi_L^2 + \psi_R^2) \, h(q^2, z). \tag{24}$$

Using the numerical solutions of (14) and (22), we numerically solve the integral in (24) as a function of q^2 . In order to compare it with the lattice QCD results, we consider a normalization of our numerical $A(q^2)$ by A(0) of the lattice data, since this initial value is not fixed in holography. Using an analytical soft-wall model, the authors in [27] proceeded by choosing A(0) from the lattice data of [10] to fix their corresponding zero momentum squared value and adjust their analytical result to these data. This can be achieved by considering a target value, say $A(0)_{\text{targ}}$ from the lattice, and then a normalized curve given by

$$A(q^2)_{\text{norm}} = A(q^2) \frac{A(0)_{\text{targ}}}{A(0)},$$
 (25)

Here we choose to compare our holographic model with the more up to date Lattice data of [12] related to the gluon contribution to $A(q^2)$. In this work, however, we extend the normalization procedure described above by choosing a range of target $A(0)_{\text{targ}}$ values that comprises the zero momentum values of [10] and [12], as well as their error bars. We choose this range as $A(0)_{\text{targ}} = 0.4 - 0.7$. Then, we perform a χ^2 minimization procedure as follows. The following χ^2 functional form is given by

$$\chi^{2} = \sum_{i=2}^{N} \frac{[A(q_{i}^{2})_{\text{norm}} - A(q_{i}^{2})_{\text{lat}})]^{2}}{\sigma^{2}}$$
(26)

where i=2 corresponds to the second value of both the normalized holographic model and the lattice value, since they are built to be equal and hence give $\chi^2=0$. N represents the total number of momenta transferred. $\sigma=0.5\,(A_{\rm upper}-A_{\rm lower})$ corresponds to the symmetric error associated with the upper and lower points of the error bars of the data from [12]. Keeping all other parameters in the model fixed, we look for the value of $A(0)_{\rm targ}$ in $A(q_i^2)_{\rm norm}$ that minimizes (26). In this context, we find $A(0)_{\rm targ}=0.628$ to be the best target value found. We point out that this target value was entered as the only degree of

freedom used in this minimization procedure. This gives $\chi^2_{\rm min} = 32.472$ and $\chi^2/{\rm ndf} = 0.984$. These results give the best-fit curve of our normalized holographic model, as illustrated in Fig. 1.

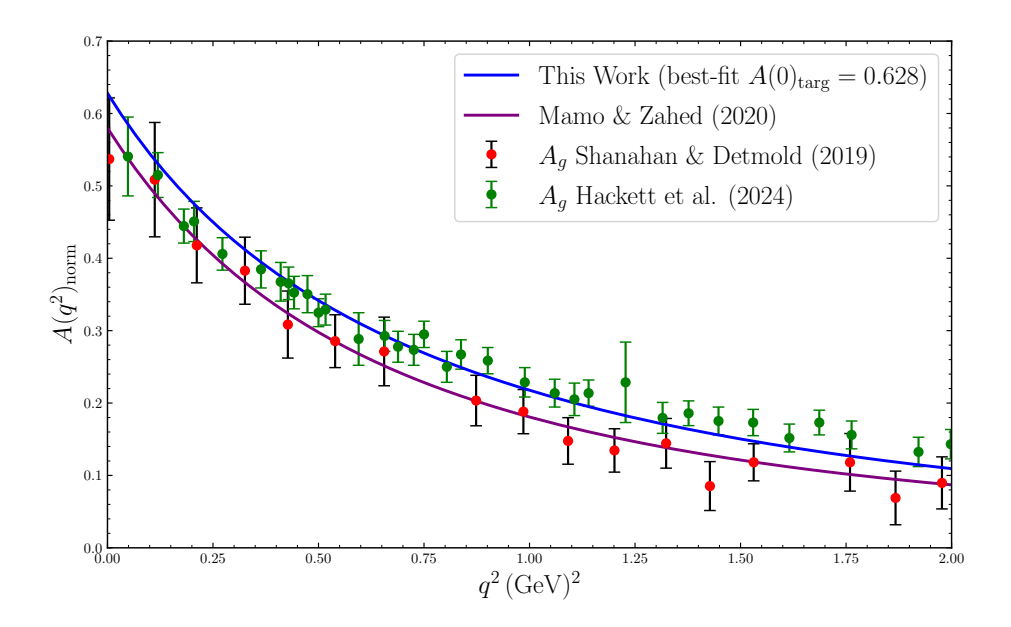


Figure 1: $A(q^2)_{norm}$ form factor adjusted to the gluon contributions of lattice data of [10] and [12]. The green dots correspond to the gluonic contribution in lattice QCD of [12], and the blue curve represents our best-fit normalized holographic form factor A . The purple curve represents the soft-wall result of Mamo & Zahed [27], compared to the lattice data of [10] (red dots).

.

The gluonic radius related to the momentum distribution is given by [2]

$$\langle r_g^2 \rangle = -6 \left(\frac{d \ln A(q^2)_{\text{norm}}}{d q^2} \right) \bigg|_{q=0} = (0.59 \,\text{fm})^2.$$
 (27)

B. $D(q^2)$ form factor

To obtain C, we must contract (18) with $\eta_{\mu\nu}$, in such a way as to extract the term proportional to q^2 , resulting in

$$C(q^2) = \frac{1}{2} \int dz \, e^{-5 \mathcal{A}(z)} H(q^2, z) \, \psi_L \, \psi_R.$$
 (28)

From the numerical integration of (28), one can calculate the form factor D defined by $D(q^2) \equiv 4 C(q^2)$. We perform the same normalization and χ^2 minimization procedure for $D(q^2)$. Similarly to $A(0)_{\text{targ}}$, we choose to restrict the target D(0) in a normalized $D(q^2)_{\text{norm}}$ to the range $D(0)_{\text{targ}} = (-1.5) - 0.0$, in which most of the lattice data from [12] lie. The resulting best target value $D(0)_{\text{targ}}$ is found to be $D(0)_{\text{targ}} = -1.192$. The resulting fit to the lattice data of [12] is illustrated in Fig. 2. We can notice that we get close to the QCD data of the lattice, but the fit is not as good as that achieved for the form factor A, especially for the high momenta transferred q^2 . Indeed, the minimization procedure described above, when applied here to $D(q^2)_{\text{norm}}$ with a target $D(0)_{\text{targ}}$, gives $\chi^2_{\text{min}} = 64.219$ with $\chi^2/\text{ndf} = 4.281$, which quantitatively states that the model deviates a considerable amount from the data considered. In fact, this seems to be a common feature shared between bottom-up holographic models such as the one used in this work and the soft-wall model considered in [27]. However, even though there is this discrepancy between our holographic model and the data considered for comparison, we can still explore the fact that its trend qualitatively follows the gluon lattice data of [10] and [12] to study the mechanical properties of the proton, such as the pressure and shear distributions in this model.

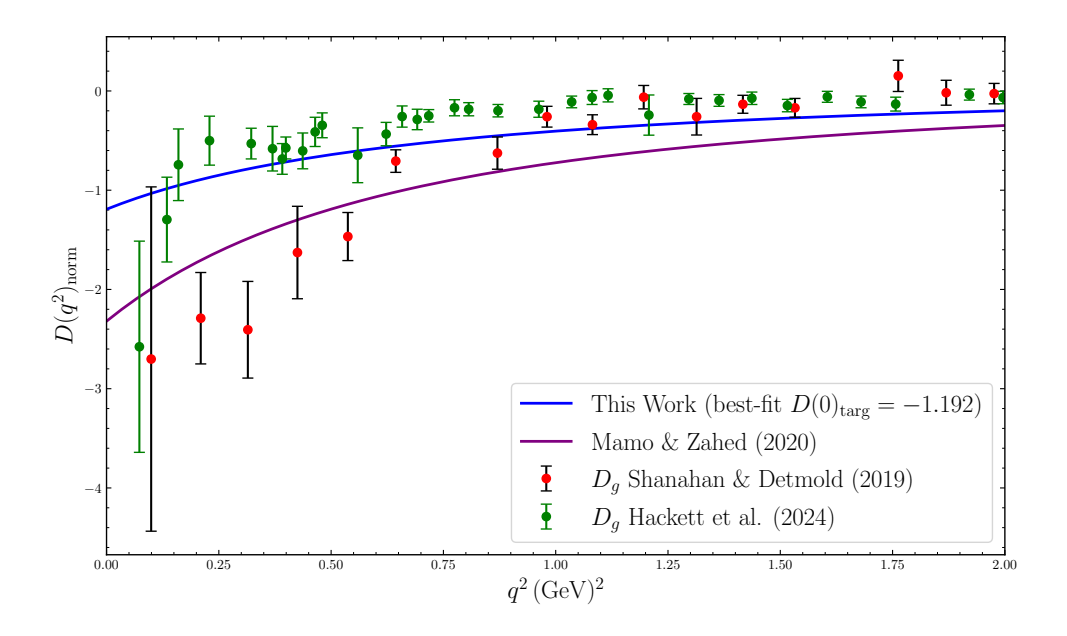


Figure 2: Holographic $D(q^2)_{norm}$ form factor from deformed AdS model (blue curve) compared to gluon lattice data of [12] (green dots). The purple curve corresponds to the soft-wall model of [27], which compares to the lattice data of [10] (red dots).

IV. PRESSURE, SHEAR, AND ENERGY DISTRIBUTIONS

Pressure and shear distributions in the system can be probed by Fourier transforming $D(q^2)$ to position space

$$\tilde{D}(r) = \int \frac{d^3q}{2 \, m \, (2\pi)^3} e^{-i \, q \cdot r} D(q^2)_{\text{norm}}.$$
(29)

This is because these distributions can be formulated in terms of $\tilde{D}(r)$ according to [2]

$$p(r) = \frac{1}{6m} \frac{1}{r^2} \frac{d}{dr} \left(r^2 \frac{d}{dr} \tilde{D}(r) \right), \tag{30}$$

$$s(r) = -\frac{r}{4m} \frac{d}{dr} \left(\frac{1}{r} \frac{d}{dr} \tilde{D}(r) \right), \tag{31}$$

with $m = M_p$ the proton mass. For numerical convenience, instead of using the numerical result for $D(q^2)_{\text{norm}}$, we use a dipole approximation to it, which is well behaved when computing its Fourier transform. We consider

$$D(q^2) = \frac{D_0}{\left(1 + \frac{q^2}{\Lambda^2}\right)^2},\tag{32}$$

where D_0 and Λ are free parameters. A very good fit to our numerical result $D(q^2)_{\text{norm}}$ is found with $D_0 = -1.196$ and $\Lambda = 1.165 \,\text{GeV}$. The pressure and shear distributions are shown by Figures 3 and 4.

One can also obtain the mechanical radius associated to those distributions, given by [2]

$$\langle r_{\text{mech}}^2 \rangle = \frac{6}{\Lambda^2} = (0.42 \,\text{fm})^2.$$
 (33)

These results are comparable with experimental results in [1] and lattice QCD ones, as in [11].

One can notice from these predictions that the strong force behaves as a repulsive force in the inner regions of the proton, whereas it behaves as a confining force in its outer regions. These positive and negative pressure regions present in Fig. 3 integrate to 2.31×10^{-6} GeV, which, within the precision of our calculation, is numerically consistent with the von Laue stability condition [56]

$$\int_0^\infty r^2 p(r) dr = 0, \tag{34}$$

that describes how internal pressure forces balance inside a composed particle, such as a proton. The shear distribution follows the pressure along the way, increasing as the pressure

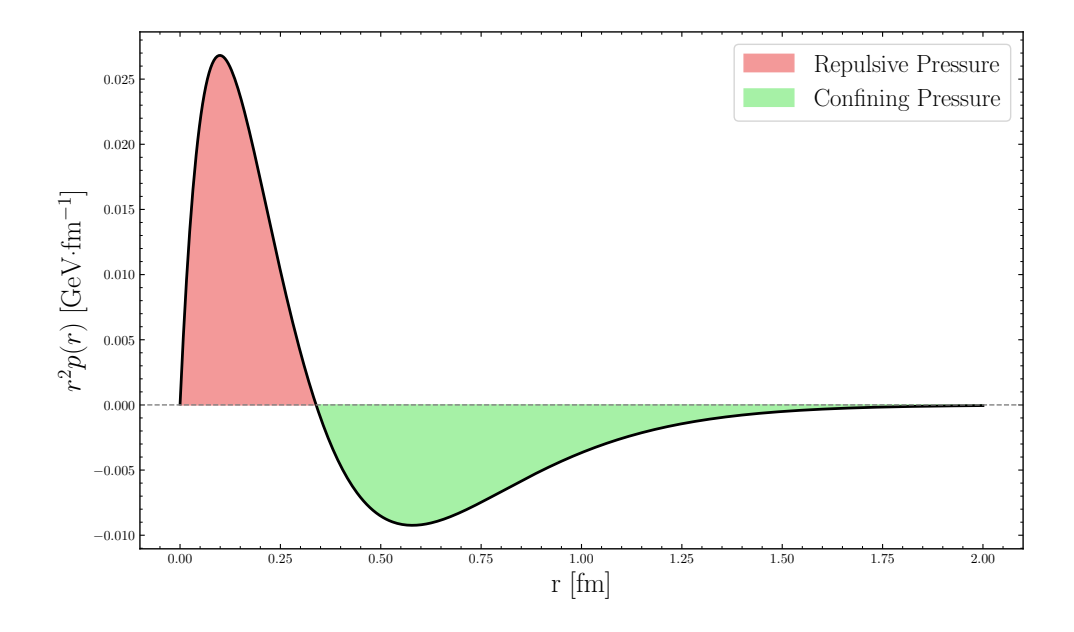


Figure 3: Pressure distribution from the dipole approximation (32), with a repulsive (red) and confining (green) pressure regions.

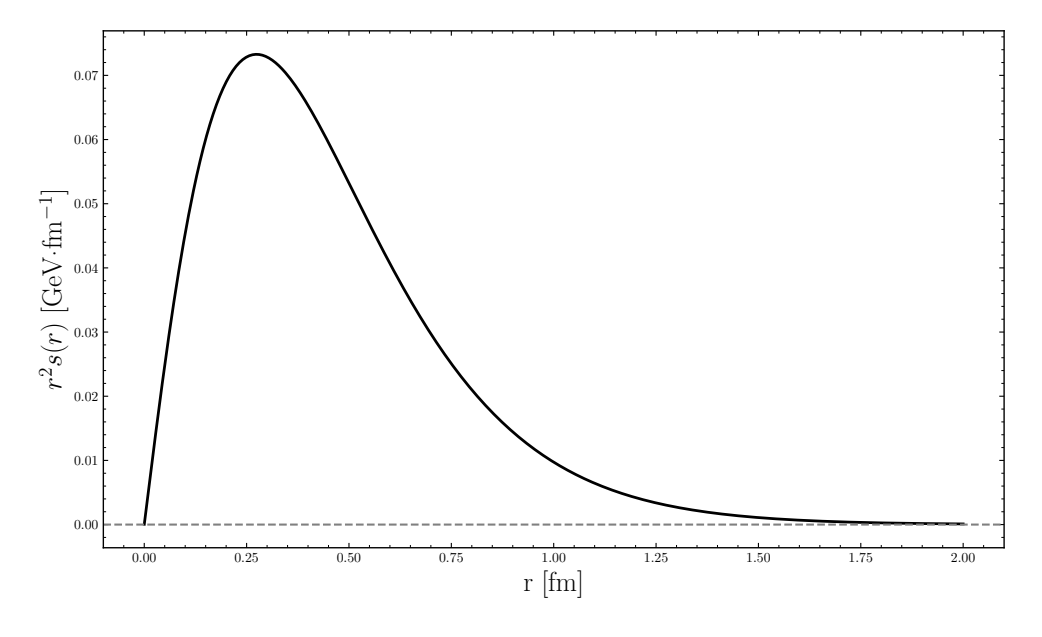


Figure 4: Shear distribution from the dipole approximation (32).

is repulsive and decreasing as it becomes more confining, acting sideways to keep the system balanced and stable. This picture can be further supported by exploring tangential and normal forces in the proton, which we are going to explore in the next section.

The energy distribution in the system is obtained by

$$\epsilon(r) = m \left[A(q^2) + \frac{q^2(D(q^2) + A(q^2) - 2B(q^2))}{4m^2} \right]_{FT}.$$
 (35)

where FT stands for Fourier transform. Here, the A and D form factors represent our normalized ones obtained in III and, in our case, B = 0. We also need to obtain an approximation to our numerical $A(q^2)_{\text{norm}}$ to compute the Fourier transform above, and again consider a dipole parameterization of the form

$$A(q^2) = \frac{A_0}{\left(1 + \frac{q^2}{\lambda^2}\right)},\tag{36}$$

with A_0 and λ free parameters. The best approximation to our numerical $A(q^2)_{\text{norm}}$ is found with $A_0 = 0.627$ and $\lambda = 1.186 \,\text{GeV}$. Hence, the resulting energy density can be computed and is displayed in Fig. 5

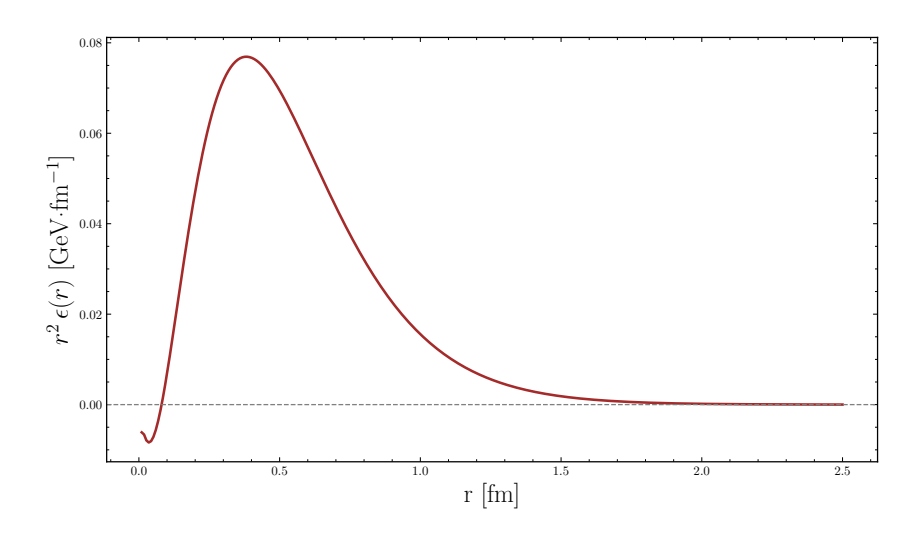


Figure 5: Energy distribution from the dipole approximations (32) and (36).

This energy distribution is very similar to that obtained in lattice QCD by [12].

V. NORMAL AND TANGENTIAL FORCES

Following [2], we consider a slice of the proton defined in spherical coordinates by $\theta = \pi/2$. The forces acting on the infinitesimal area element $d\mathbf{S} = dS_n \, \mathbf{e}_n + dS_\theta \, \mathbf{e}_\theta + dS_\phi \, \mathbf{e}_\phi +$ of the slice are

$$\frac{dF_n}{dS_n} = \frac{2}{3}s(r) + p(r), \quad \frac{dF_\theta}{dS_\theta} = \frac{dF_\phi}{dS_\phi} = -\frac{1}{3}s(r) + p(r), \tag{37}$$

with the tangential forces being equal when considering the proton as a spherical symmetrical system. Then, the normal and tangential forces on a spherical shell of radius r in the proton

are F_n and F_t ,

$$F_n = 4\pi r^2 \left[\frac{2}{3} s(r) + p(r) \right], \quad F_t = 4\pi r^2 \left[-\frac{1}{3} s(r) + p(r) \right],$$
 (38)

which are displayed in Fig. 6. Regarding the normal force, its positive values correspond

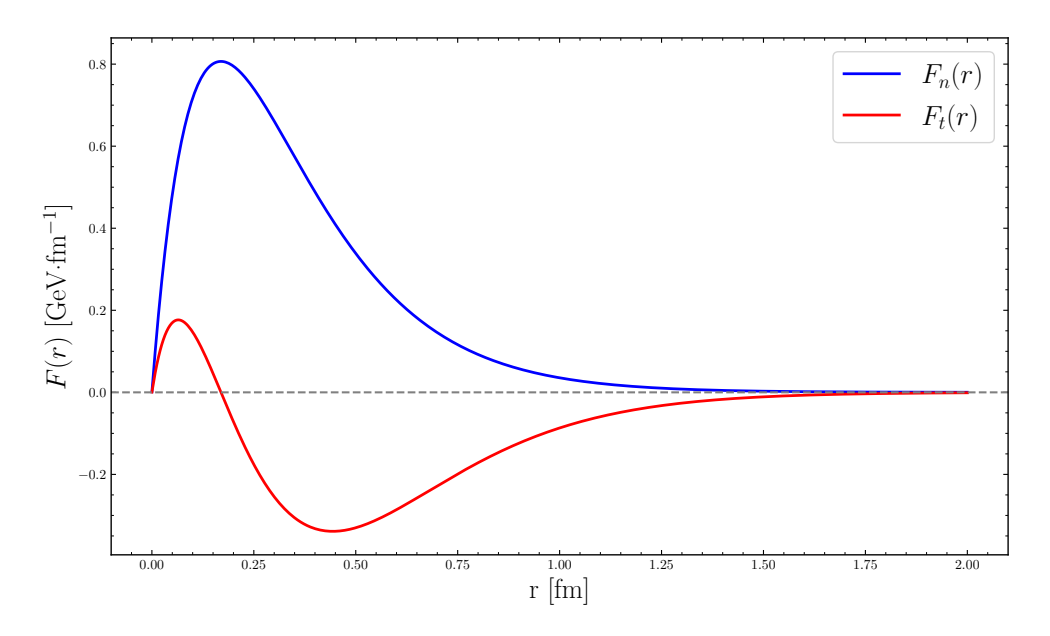


Figure 6: Normal and tangential forces on a spherical shell of radius r in the nucleon.

to stretching in the system, which is present mainly in the inner regions of the proton. The change in sign of the tangential forces acts to counterbalance any possible squeeze from the confining pressure so that it averages to zero. This behavior of the tangential forces can also be seen from the force field point of view, as illustrated by Fig. 7. A force field visualization for $F_n(r)$ is also displayed in Fig. 8.

VI. CONCLUSIONS

In the present work, we employ the deformed AdS background holographic model to describe gravitational form factors of the proton and explore some of its mechanical properties based on the D term, focusing on the contribution of the gluon to them. We find a very good agreement between our prediction for the gluonic form factor A and the recent lattice QCD computation performed in [12], using a normalization procedure to fit A(0) to the lattice result with a target $A(0)_{\text{targ}}$ that minimizes the χ^2 measure of the difference between our model prediction and the lattice data. Its trend is also compared to the previous

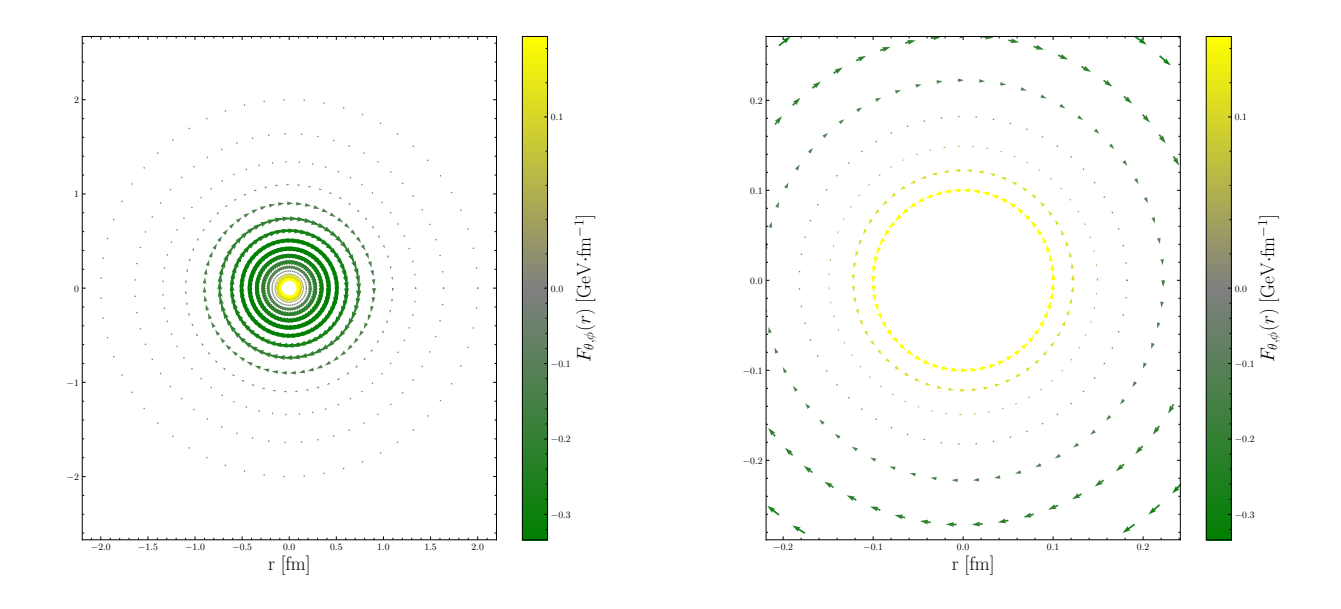


Figure 7: Force field visualization of the tangential forces F_{θ} and F_{ϕ} as functions of r. The left panel displays the full profile of these forces. The right panel zooms in into the inner region where the sign of the forces changes.

holographic result of [27] as well as to the previous lattice data of [10]. The same approach is carried out for the gluonic term D, resulting, in this case, in a qualitative agreement between our model and the lattice data of [12], whose behavior draws a particular shape not fully captured by the holographic model used in this work. However, we remark that those results were obtained numerically in all the steps present in their calculations, in contrast to previous holographic results using the soft-wall model in [20, 27], which use analytical solutions to form factors. The general agreement between the numerical results in our work, which are also in the ballpark of the results present in [10, 27], and the lattice results of [12], shows that this model is capable of capturing features present in both the lattice QCD literature and previous holographic models.

From the D term, since its trend follows the behavior present in the lattice results, we can explore how the model describes some mechanical properties of the nucleon. Using a dipole approximation to our numerical result, which is better suited for the calculation of the Fourier transform of D(r) and A(r), we can compute the pressure and shear distributions inside the proton, which balance each other to keep the system stable. This is supported by the small value of the integral $\int r^2 p(r) dr = 2.31 \times 10^{-6} \,\text{GeV}$ in our approximation, which

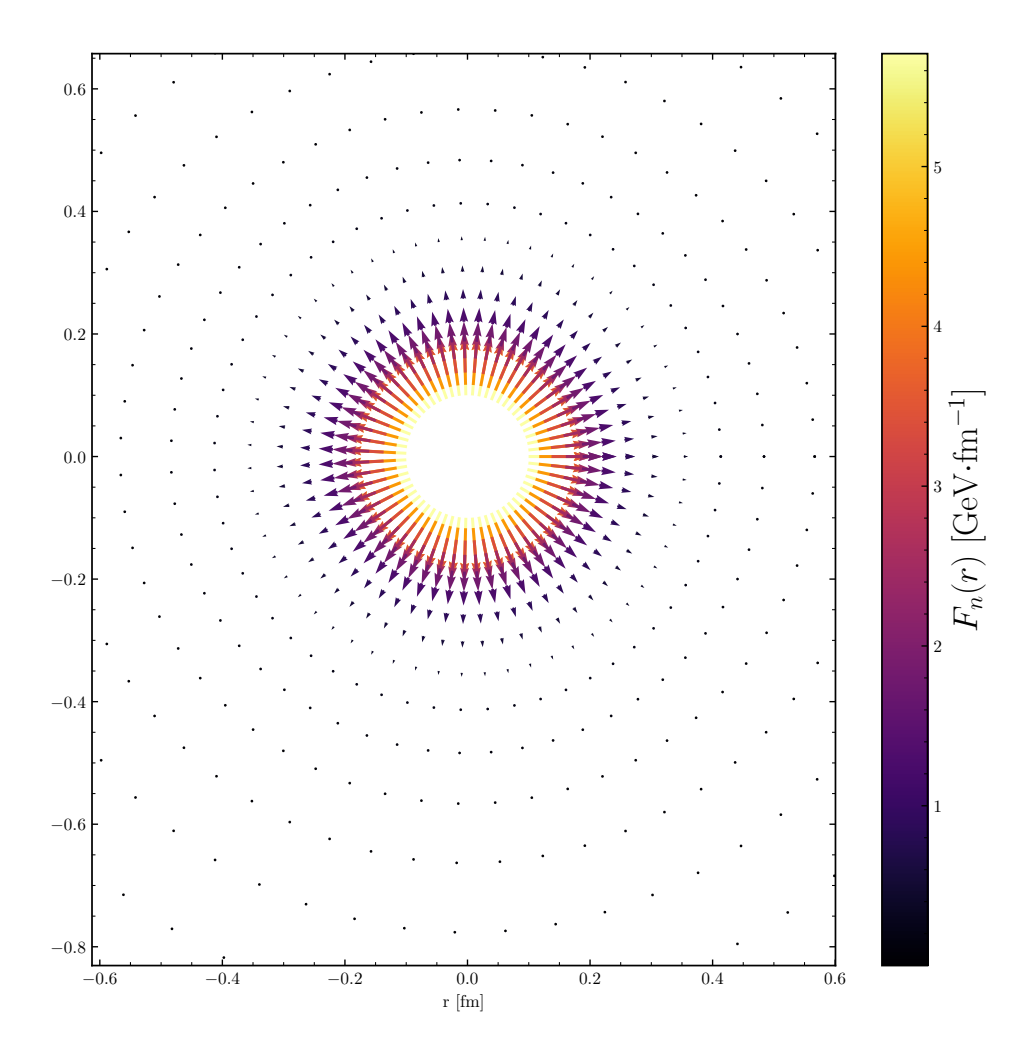


Figure 8: Force field visualization of the normal force $F_n(r)$ inside the proton.

should be zero in the exact case. We are also able to evaluate the energy density in the proton using a dipole approximation to $A(q^2)_{\text{norm}}$. The results follow similar trends present in the literature, e.g., such as those in [1, 2, 4, 7, 11, 27, 30]. However, the mechanical radius associated with these distributions is smaller than the ones found in these works. From pressure and shear distributions, internal forces are also investigated, presenting a similar behavior appearing in this literature.

We plan to further extend these discussions to the case of the pion in the present holographic model in a future work, since this hadron's GFFs were less explored in previous holographic models, and lattice data are also available to be compared with. We hope that this work can help future experiments to be carried out by the EIC in the near future, by supporting the predictions to the internal forces acting inside the proton and how the strong nuclear force manifests in hadronic systems.

ACKNOWLEDGMENTS

We would like to thank Jorge Noronha for enlightening discussions. A. N. acknowledges the support by the Brazilian National Council for Scientific and Technological Development under grant No. 176343/2025-3. HBF is partially supported by Conselho Nacional de Desenvolvimento Científico e Tecnológico (CNPq) under grant 310346/2023-1, and Fundação Carlos Chagas Filho de Amparo à Pesquisa do Estado do Rio de Janeiro (FAPERJ) under grant E-26/204.095/2024.

[1] V. D. Burkert, L. Elouadrhiri, and F. X. Girod, Nature **557**, 396 (2018).

- [2] M. V. Polyakov and P. Schweitzer, Int. J. Mod. Phys. A 33, 1830025 (2018), arXiv:1805.06596 [hep-ph].
- [3] A. Deur, S. J. Brodsky, and G. F. De Téramond, Rept. Prog. Phys. **82**, 076201 (2019), arXiv:1807.05250 [hep-ph].
- [4] C. Lorcé, H. Moutarde, and A. P. Trawiński, Eur. Phys. J. C 79, 89 (2019), arXiv:1810.09837 [hep-ph].
- [5] V. D. Burkert, L. Elouadrhiri, F. X. Girod, C. Lorcé, P. Schweitzer, and P. E. Shanahan, Rev. Mod. Phys. 95, 041002 (2023), arXiv:2303.08347 [hep-ph].
- [6] M. Gell-Mann, Phys. Rev. **125**, 1067 (1962).
- [7] V. D. Burkert, L. Elouadrhiri, and F. X. Girod, (2021), arXiv:2104.02031 [nucl-ex].
- [8] A. Accardi et al., Eur. Phys. J. A 52, 268 (2016), arXiv:1212.1701 [nucl-ex].
- [9] C. Alexandrou, M. Constantinou, K. Hadjiyiannakou, K. Jansen, C. Kallidonis, G. Koutsou, and A. Vaquero Avilés-Casco, PoS **DIS2018**, 148 (2018), arXiv:1807.11214 [hep-lat].
- [10] P. E. Shanahan and W. Detmold, Phys. Rev. D **99**, 014511 (2019), arXiv:1810.04626 [hep-lat].
- [11] P. E. Shanahan and W. Detmold, Phys. Rev. Lett. 122, 072003 (2019), arXiv:1810.07589
 [nucl-th].
- [12] D. C. Hackett, D. A. Pefkou, and P. E. Shanahan, Phys. Rev. Lett. 132, 251904 (2024), arXiv:2310.08484 [hep-lat].

- [13] J. M. Maldacena, Adv. Theor. Math. Phys. 2, 231 (1998), arXiv:hep-th/9711200.
- [14] S. S. Gubser, I. R. Klebanov, and A. M. Polyakov, Phys. Lett. B 428, 105 (1998), arXiv:hep-th/9802109.
- [15] E. Witten, Adv. Theor. Math. Phys. 2, 253 (1998), arXiv:hep-th/9802150.
- [16] Z. Abidin and C. E. Carlson, Phys. Rev. D 77, 095007 (2008), arXiv:0801.3839 [hep-ph].
- [17] Z. Abidin and C. E. Carlson, Phys. Rev. D 77, 115021 (2008), arXiv:0804.0214 [hep-ph].
- [18] S. J. Brodsky and G. F. de Teramond, Phys. Rev. D 78, 025032 (2008), arXiv:0804.0452 [hep-ph].
- [19] Z. Abidin and C. E. Carlson, Phys. Rev. D 78, 071502 (2008), arXiv:0808.3097 [hep-ph].
- [20] Z. Abidin and C. E. Carlson, Phys. Rev. D 79, 115003 (2009), arXiv:0903.4818 [hep-ph].
- [21] N. Anderson, S. K. Domokos, J. A. Harvey, and N. Mann, Phys. Rev. D 90, 086010 (2014), arXiv:1406.7010 [hep-ph].
- [22] D. Chakrabarti, C. Mondal, and A. Mukherjee, Phys. Rev. D 91, 114026 (2015), arXiv:1505.02013 [hep-ph].
- [23] C. Mondal, Eur. Phys. J. C **76**, 74 (2016), arXiv:1511.01736 [hep-ph].
- [24] C. Mondal, D. Chakrabarti, and X. Zhao, Eur. Phys. J. A 53, 106 (2017), arXiv:1705.05808
 [hep-ph].
- [25] N. Kumar, C. Mondal, and N. Sharma, Eur. Phys. J. A 53, 237 (2017), arXiv:1712.02110 [hep-ph].
- [26] A. Watanabe and M. Huang, Phys. Lett. B 788, 256 (2019), arXiv:1809.02515 [hep-ph].
- [27] K. A. Mamo and I. Zahed, Phys. Rev. D 101, 086003 (2020), arXiv:1910.04707 [hep-ph].
- [28] T. M. Aliev, K. Şimşek, and T. Barakat, Phys. Rev. D 103, 054001 (2021), arXiv:2009.07926 [hep-ph].
- [29] D. Chakrabarti, C. Mondal, A. Mukherjee, S. Nair, and X. Zhao, Phys. Rev. D 102, 113011 (2020), arXiv:2010.04215 [hep-ph].
- [30] K. A. Mamo and I. Zahed, Phys. Rev. D 103, 094010 (2021), arXiv:2103.03186 [hep-ph].
- [31] G. Karapetyan, Eur. Phys. J. Plus 137, 590 (2022), arXiv:2112.11359 [nucl-th].
- [32] Z. Liu, W. Xie, F. Sun, S. Li, and A. Watanabe, Phys. Rev. D 106, 054025 (2022), arXiv:2202.08013 [hep-ph].
- [33] M. Allahverdiyeva and S. Mamedov, Eur. Phys. J. C 83, 447 (2023), arXiv:2302.03383 [hep-ph].

- [34] S. Mamedov, M. Allahverdiyeva, and N. Akbarova, Eur. Phys. J. C 85, 361 (2025), arXiv:2412.17407 [hep-ph].
- [35] J. Deng and D. Hou, Phys. Rev. D 112, 036011 (2025), arXiv:2502.00771 [nucl-th].
- [36] A. Sain, P. Choudhary, B. Gurjar, C. Mondal, D. Chakrabarti, and A. Mukherjee, Phys. Rev. D 111, 094011 (2025), arXiv:2503.12574 [hep-ph].
- [37] J. Polchinski and M. J. Strassler, Phys. Rev. Lett. 88, 031601 (2002), arXiv:hep-th/0109174.
- [38] H. Boschi-Filho and N. R. F. Braga, JHEP **05**, 009 (2003), arXiv:hep-th/0212207.
- [39] H. Boschi-Filho and N. R. F. Braga, Eur. Phys. J. C 32, 529 (2004), arXiv:hep-th/0209080.
- [40] G. F. de Teramond and S. J. Brodsky, Phys. Rev. Lett. 94, 201601 (2005), arXiv:hep-th/0501022.
- [41] J. Erlich, E. Katz, D. T. Son, and M. A. Stephanov, Phys. Rev. Lett. 95, 261602 (2005), arXiv:hep-ph/0501128.
- [42] H. Boschi-Filho, N. R. F. Braga, and H. L. Carrion, Phys. Rev. D 73, 047901 (2006), arXiv:hep-th/0507063.
- [43] A. Karch, E. Katz, D. T. Son, and M. A. Stephanov, Phys. Rev. D 74, 015005 (2006), arXiv:hep-ph/0602229.
- [44] S. J. Brodsky and G. F. de Teramond, Phys. Rev. Lett. 96, 201601 (2006), arXiv:hep-ph/0602252.
- [45] J. Erdmenger, N. Evans, I. Kirsch, and E. Threlfall, Eur. Phys. J. A 35, 81 (2008), arXiv:0711.4467 [hep-th].
- [46] S. J. Brodsky, G. F. de Teramond, H. G. Dosch, and J. Erlich, Phys. Rept. 584, 1 (2015), arXiv:1407.8131 [hep-ph].
- [47] T. Sakai and S. Sugimoto, Prog. Theor. Phys. 113, 843 (2005), arXiv:hep-th/0412141.
- [48] T. Sakai and S. Sugimoto, Prog. Theor. Phys. 114, 1083 (2005), arXiv:hep-th/0507073.
- [49] H. Hata, T. Sakai, S. Sugimoto, and S. Yamato, Prog. Theor. Phys. 117, 1157 (2007), arXiv:hep-th/0701280.
- [50] O. Andreev and V. I. Zakharov, Phys. Rev. D 74, 025023 (2006), arXiv:hep-ph/0604204.
- [51] E. Folco Capossoli, M. A. Martín Contreras, D. Li, A. Vega, and H. Boschi-Filho, Chin. Phys. C 44, 064104 (2020), arXiv:1903.06269 [hep-ph].
- [52] E. Folco Capossoli, M. A. Martín Contreras, D. Li, A. Vega, and H. Boschi-Filho, Phys. Rev. D 102, 086004 (2020), arXiv:2007.09283 [hep-ph].

- [53] M. A. Martin Contreras, E. Folco Capossoli, D. Li, A. Vega, and H. Boschi-Filho, Nucl. Phys. B 977, 115726 (2022), arXiv:2104.04640 [hep-ph].
- [54] M. A. M. Contreras, E. F. Capossoli, D. Li, A. Vega, and H. Boschi-Filho, Phys. Lett. B 822, 136638 (2021), arXiv:2108.05427 [hep-ph].
- [55] A. d. C. P. d. Nascimento and H. Boschi-Filho, Phys. Rev. D 108, 106008 (2023), arXiv:2306.17315 [hep-th].
- [56] M. Laue, Annalen der Physik **340**, 524 (1911).